The Emergence of Multiple Robust Zonal Jets from Freely Evolving, Three-Dimensional Stratified Geostrophic Turbulence with Applications to Jupiter

KUNIO M. SAYANAGI*
Comparative Planetology Laboratory, University of Louisville, Louisville, Kentucky

ADAM P. SHOWMAN
Department of Planetary Sciences, Lunar and Planetary Laboratory, The University of Arizona, Tucson, Arizona

TIMOTHY E. DOWLING
Comparative Planetology Laboratory, University of Louisville, Louisville, Kentucky

(Manuscript received 6 July 2007, in final form 3 June 2008)

ABSTRACT

Three-dimensional numerical simulations of freely evolving stratified geostrophic turbulence on the β plane are presented as a simplified model of zonal jet formation on Jupiter. This study samples the parameter space that covers the low, middle, and high latitudes of Jupiter by varying the central latitude of the β plane. The results show that robust zonal jets can emerge from initial small-scale random turbulence through the upscale redistribution of the kinetic energy in the spectral space. The resulting flow's sensitivities to the flow's deformation radius L_D and the two-dimensional Rhines length $L_\beta = \sqrt{U/\beta}$ (U is the characteristic turbulence velocity and β is the meridional gradient of the planetary vorticity) are tested, revealing that whether the outcome of the upscale energy transfer becomes dominated by jets or vortices depends on the relative values of L_D and L_β. The values of L_β and L_D are varied by tuning the β-plane parameters, and it is found that the flow transitions from a jet-dominated regime in $L_\beta \lesssim L_D$ to a vortical flow in $L_\beta \gtrsim L_D$. A height-to-width ratio equal to f/N, the Coriolis parameter divided by the Brunt–Väisälä frequency, has previously been established for stable vortices, and this paper shows that this aspect ratio also applies to the zonal jets that emerge in these simulations.

1. Introduction

Spacecraft observations of Jupiter reveal ~30 zonal jets at the cloud level. In the equatorial region, a fast, broad, eastward jet dominates the flow flanked by westward jets to the north and south. Vortices are absent in the equatorial region roughly between ±20° latitudes. Outside of the equatorial region, numerous zonal jets exist up to ±60° latitudes. Many of the jets contain stable vortices that drift in the east–west direction at speeds slightly different from the background zonal flow. The jets equatorward of 60° latitudes, including the equatorial region, are extremely steady even though they violate the barotropic stability criterion at some latitudes. The spatial steadiness is signified by the observation that the longitudinal wind speed dependence within a jet is much smaller than the variations of the zonal mean zonal wind in latitude (Limaye 1986). Comparing the zonal mean wind profiles from the *Voyager* measurements in 1979 with the *Cassini* measurements in 2000 illustrates the steadiness of the zonal jets in time, in which only minor changes in the locations and the speeds of those jets are found (Porco et al. 2003). Poleward of ~60° latitude, both the visible appearances and the dynamical characteristics change dramatically from the lower latitudes. Whereas the low- to mid-latitude regions are characterized by alternating dark and bright bands whose boundaries correspond to the peaks of the zonal jets, the high-latitude regions lack clear banding and are instead marked by countless small vortices. *Cassini* observations of the northern high latitudes of Jupiter reveal a wind flow dominated

* Current affiliation: Division of Geological and Planetary Sciences, California Institute of Technology, Pasadena, California.

Corresponding author address: Kunio M. Sayanagi, Division of Geological and Planetary Sciences, California Institute of Technology, MC 170-25, 1200 E. California Blvd., Pasadena, CA 91125.
E-mail: sayanagi@gps.caltech.edu

DOI: 10.1175/2008JAS2558.1

by numerous vortices ranging in size from the limit of image resolution to thousands of kilometers (Porco et al. 2003). A comprehensive Jovian atmospheric dynamics model must explain these three dynamical wind regimes: the vortex-free equatorial region with a fast, broad, eastward jet, the middle latitudes where stable vortices are embedded in the numerous robust zonal jets that violate the barotropic stability criterion, and the vortex-dominated flow in the high latitudes.

The tendency for small-scale random turbulence on a rotating spherical surface to self-organize into zonally elongated structures lays the foundation of a promising hypothesis for Jovian zonal jet formation. This topic—turbulence on a rotating spherical surface, including geostrophic turbulence—has been extensively reviewed by Rhines (1979, 1994), Vasavada and Showman (2005), and Galperin et al. (2006). In 2D fluid flow, it is well known that kinetic energy tends to be transferred from small-scale features to larger scales (i.e., in the inverse direction from three-dimensional turbulence) and accumulates at the largest scale in the flow domain (Batchelor 1953). Vortex growth through vortex mergers is a manifestation of this upscale kinetic energy transfer. For a 2D flow on a rotating spherical surface, Rhines (1975) showed that the gradient of the local planetary vorticity β has an important effect on the redistribution of kinetic energy in the spectral space. Under sufficiently large β, Rhines showed that this inverse energy transfer results in structures elongated in the zonal directions with the north–south characteristic width

$$L_\beta = (U/\beta)^{1/2}, \tag{1}$$

where $\beta = df/dy$, y is northward distance, $f = 2\Omega \sin\phi$, Ω is planetary rotation rate, and ϕ is latitude. Today, this effect is called the Rhines effect, and L_β is known as the Rhines length[1] and remains an active area of investigation. There have been studies of zonal jet formation as a result of the Rhines effect using unforced (e.g., Yoden and Yamada 1993; Huang and Robinson 1998; Yoden et al. 1999) and forced flows (e.g., Chekhlov et al. 1996; Nozawa and Yoden 1997; Huang and Robinson 1998; Huang et al. 2001; Danilov and Gurarie 2004; Danilov and Gryanik 2004; Sukoriansky et al. 2007). In a study of an unforced flow, the problem is treated as an initial value problem with a prescribed flow pattern that places most of the energy in small-scale structures—the focus of the study is the subsequent redistribution of the kinetic energy in the spectral space. In a forced flow, energy is continuously added to the system at the small scale and continuously cascades through the spectral space. In both forced and unforced cases, the kinetic energy transfers predominantly toward smaller wavenumbers (i.e., toward larger length scales). The present study focuses on unforced flows on a β plane, as will be discussed in later sections.

Using quasigeostrophic (QG) models, Okuno and Masuda (2003) and Smith (2004) showed that the Rhines effect can be suppressed in the case of finite Rossby deformation radius and nonzero flow divergence. For single-layer fluid flow, the Rossby deformation radius is $L_D = \sqrt{gh}/f$, where g and h are the gravitational acceleration at the surface and depth of flow, respectively. The 2D nondivergent model, which was used in Rhines (1975) and other earlier studies, has $L_D \to \infty$. When the deformation radius is finite, Okuno and Masuda (2003) showed that the Rhines length takes the form

$$L'_\beta \approx \left(\frac{1}{L_\beta^2} - \frac{1}{L_D^2}\right)^{-1/2}. \tag{2}$$

When $L_D \ll L_\beta$, (2) shows that L'_β becomes imaginary, and Okuno and Masuda (2003) and Smith (2004) show that the Rhines effect is suppressed under such conditions. Theiss (2004) suggests that the critical latitude on Jupiter (i.e., the boundary between the jet-dominated latitudes and the vortex-dominated polar region) is marked by $L_D \approx L_\beta$.

Nonlinear simulations using the shallow-water (SW) model further demonstrate that the suppression of the Rhines effect under small L_D also occurs when the ageostrophic effects are fully included. Simulations of freely evolving (Cho and Polvani 1996; Iacono et al. 1999) and forced (Showman 2007; Scott and Polvani 2007) turbulence showed that SW flows can produce multiple zonal jets in low latitudes accompanied by vortex-dominated regions in the high latitudes. Note that under horizontally uniform stratification L_D decreases with latitude as f increases. In these simulations, a clear critical latitude divides the jets and the vortex-dominated regions. The studies also report the dominance of anticyclonic vortices over cyclones, another key Jovian flow feature. However, under Jovian conditions of small L_D, their equatorial jet becomes westward, the opposite of Jupiter, and they do not reproduce a flow regime in which small vortices are embedded in stable zonal jets. The successes of the SW studies over the 2D nondivergent cases illuminate that the horizontal flow divergence is crucial in reproducing two of the key Jovian flow features, namely, the vortex-free low latitudes and the vortex-dominated polar regions. On the other hand, the failures of the single layer models to repro-

[1] Note that the original form by Rhines is $L_\beta = \sqrt{2U/\beta}$; the form presented in (1) has become more common in recent years.

duce other Jovian characteristics, including stable vortices embedded in zonal jets, leave open the possibility that 3D effects are important in reproducing all such key features in a single model.

Our study is motivated by the aforementioned QG and SW studies showing that the Rhines effect becomes suppressed under finite deformation radius. To our knowledge, this idea has not previously been systematically tested through 3D atmospheric modeling. Although there have been studies of cloud-level Jovian jet formation in 3D using multilayer primitive equation models, their focus is largely on the effect of radiative and/or latent heat forcing (e.g., Williams 2003; Lian and Showman 2008). In such studies, the source of small-scale vorticity is baroclinic instability, and zonal jets form with their widths following the Rhines scale (Lian and Showman 2008). However, to date, we are aware of Kitamura and Matsuda (2004) as the only published study of freely evolving 3D stratified turbulence that addresses zonal jet formation from finescale random flow. Kitamura and Matsuda (2004) found that from the initial turbulence, strong circumpolar jets and weaker midlatitude jets emerge, which is not very Jupiter-like. However, their model has only two vertical levels, and the resulting jets' vertical structures are poorly resolved. Our report here extends Kitamura and Matsuda (2004)'s study by including many more layers in the vertical to permit much wider range of 3D effects.

Below, we present a full-3D primitive equation model investigation of freely evolving stratified turbulence on a β plane to show that robust zonal jets can emerge from initial finescale turbulence. Even though this is a β-plane study, we sample the parameter space associated with low, middle, and high latitudes by varying the central latitude of the β plane (section 3d). The rest of our paper is structured as follows: In section 2, we present the setup of our numerical experiments. Section 3 presents our results, which show that robust zonal jets can emerge from initial random turbulence. Section 4 analyzes the width-to-height aspect ratio of the jets that emerge in our simulations. Concluding remarks are in the final section.

2. Model setup

a. Numerical model

We use the Explicit Planetary Isentropic Coordinate (EPIC) atmosphere model by Dowling et al. (1998) to perform our numerical experiments. The model solves the hydrostatic primitive equations with the potential temperature θ as the vertical coordinate. Because our main focus here is to study the processes that may be involved in the formation of Jupiter's zonal jets, many of our baseline parameters represent their respective values for Jupiter, including the gravitational acceleration and the ranges of variations for the Coriolis parameter and its gradient. We also initialize the background vertical thermal structure by setting the 200-mb level temperature to be 110 K to obtain a scale height similar to the Jovian condition. At the same time, we also reduce the number of free parameters by simplifying the model atmosphere.

First, our simulations in this study are run in the β-plane approximation, which is a linear approximation of the Coriolis parameter

$$f(y) = \beta y + f_0, \tag{3}$$

where f_0 is the baseline Coriolis parameter. Second, the model atmosphere is stratified such that it has a constant background Brunt–Väisälä frequency N throughout the model domain. We forego the stratosphere, in which the static stability is substantially higher than in the troposphere, because in 3D the deformation radius of the flow depends on the stratification, and thus large variations in N within a simulation domain introduce complications in interpreting our results. Third, our simulations do not contain any explicit forcing (except for the numerical stability terms noted later). We treat our study as a pure initial value problem and do not take radiation into account even though our $\gtrsim$500-day-long simulations are comparable to or longer than the radiative time scales at some altitudes on Jupiter. Finally, we incorporate the ideal gas equation of state, with the heat capacity with constant pressure c_p = 11 290 J kg^{-1} K^{-1} and the specific gas constant R = 3500 J kg^{-1} K^{-1}.

Most of our simulations have a horizontal domain size of 30 000 km $\times$ 30 000 km with the north–south $\times$ east–west grid resolution of 128 $\times$ 128. The number of layers is varied from 12 to 36 (full details are given in Table 1). The north–south lateral boundaries have the free-slip (i.e., stress-free) condition and the east–west boundaries are periodic. We ensure that the domain size is substantially larger than the resulting widths of the jets and radii of the vortices. We tested the sensitivities of our results to the horizontal resolution and the domain size by doubling the horizontal model domain and then, in a separate simulation, doubling the horizontal model resolution while keeping the domain size the same as the nominal cases. These sensitivity tests revealed that the width and spacing of the jets that emerge are not affected by the model domain and resolution.

The vertical domain height and resolution for each simulation are listed in Table 1. The vertical resolutions are chosen such that the vortices of the smallest radius

TABLE 1. List of simulations.

Identifier	β (m^{-1} s^{-1})	f_0 (s^{-1})	N (s^{-1})	Simulation domain height (SH)[1,2]	Vertical resolution (layers)[3]	Number of sponge layers	Layer spacing (SH)[1]	Initial vortex height (SH)[1]	Resulting flow[4]
Nominal case									
$\beta 30 f 30$-H	4.26×10^{-12}	1.76×10^{-4}	0.005	2.9	24	6	0.17	0.5	Zonal jets
β sensitivity test									
$\beta 15 f 30$-H	4.75×10^{-12}	1.76×10^{-4}	0.005	2.9	24	6	0.17	0.5	Zonal jets
$\beta 60 f 30$-H	2.46×10^{-12}	1.76×10^{-4}	0.005	2.9	24	6	0.17	0.5	Vortices between zonal jets
$\beta 80 f 30$-H	8.55×10^{-13}	1.76×10^{-4}	0.005	2.9	24	6	0.17	0.5	Vortices with zonal flow
f sensitivity test									
$\beta 30 f 15$-H	4.26×10^{-12}	9.11×10^{-5}	0.005	2.9	24	6	0.17	0.5	Zonal jets
$\beta 30 f 60$-H	4.26×10^{-12}	3.05×10^{-4}	0.005	2.9	24	6	0.17	0.5	Vortices between zonal jets
$\beta 30 f 80$-H	4.26×10^{-12}	3.47×10^{-4}	0.005	2.9	24	6	0.17	0.5	Vortices with zonal flow
Latitude sensitivity test—High static stability									
$\beta 15 f 15$-H	4.75×10^{-12}	9.11×10^{-5}	0.005	2.9	24	6	0.17	0.5	Zonal jets
$\beta 60 f 60$-H	2.46×10^{-12}	3.05×10^{-4}	0.005	2.9	24	6	0.17	0.5	Vortices between zonal jets
$\beta 80 f 80$-H	8.55×10^{-13}	3.47×10^{-4}	0.005	2.9	24	6	0.17	0.5	Vortex dominated
Latitude sensitivity test—Low static stability									
$\beta 15 f 15$-L	4.75×10^{-12}	9.11×10^{-5}	0.001	6.0	12	2	0.73	1.5	Zonal jets
$\beta 30 f 30$-L	4.26×10^{-12}	1.76×10^{-4}	0.001	6.0	12	2	0.73	1.5	Vortices with zonal flow
$\beta 60 f 60$-L	2.46×10^{-12}	3.05×10^{-4}	0.001	6.0	12	2	0.73	1.5	Vortex dominated
$\beta 80 f 80$-L	8.55×10^{-13}	3.47×10^{-4}	0.001	6.0	12	2	0.73	1.5	Vortex dominated
Deep domain simulations									
$\beta 30 f 15$-D	4.26×10^{-12}	9.11×10^{-5}	0.005	5.0	36	6	0.17	0.5	Zonal jets
$\beta 30 f 30$-D	4.26×10^{-12}	1.76×10^{-4}	0.005	5.0	36	6	0.17	0.5	Zonal jets
$\beta 30 f 60$-D	4.26×10^{-12}	3.05×10^{-4}	0.005	5.0	36	6	0.17	0.5	Vortices with zonal jets
$\beta 30 f 80$-D	4.26×10^{-12}	3.47×10^{-4}	0.005	5.0	36	6	0.17	0.5	Vortices with zonal jets

[1] SH stands for scale height.
[2] The simulation domain height shown here is the height of the active (i.e., nonsponge) domain.
[3] The number of layers here includes the sponge layers.
[4] Here, we call a zonal feature a jet when both of the following criteria are satisfied: $Z > 2.5$ and $|\overline{u}| > 0.5$ m s^{-1}. A zonal flow is a feature that extends throughout the domain without reversing direction though it does not satisfy at least one of these criteria.

that can be accommodated in our model can be resolved in the vertical, following Dritschel and de la Torre Juárez's (1996) results, who found that vortices with height-to-radius ratio larger than $3f/N$ are unstable, and we set the vertical and horizontal resolutions (Δz and Δx, respectively) so that $\Delta z/\Delta x < 3f/N$. The vertical domain height is set to be as tall as computationally feasible while maintaining sufficient vertical resolution, as explained above. The bottommost model layer is a nonevolving abyssal layer representing the deep convective interior of a gas-giant planet. All wind components are zero in the abyssal layer in our simulations. It is possible that nonzero abyssal flows significantly affect the overlying flow. However, this would introduce another free parameter, namely, the width of the abyssal jets. We avoid this complication by setting the abyssal flow to be zero.

To ensure numerical stability, we add sixth-order hyperviscosity throughout the domain and sponge layers at the top of the model. The sponge layers prevent waves from unphysically reflecting at the model top. We configure the sponge such that the lowest sponge layer is placed at the ~700-mb level and their effects are minimal for layers below the 1000-mb (1-bar) level.

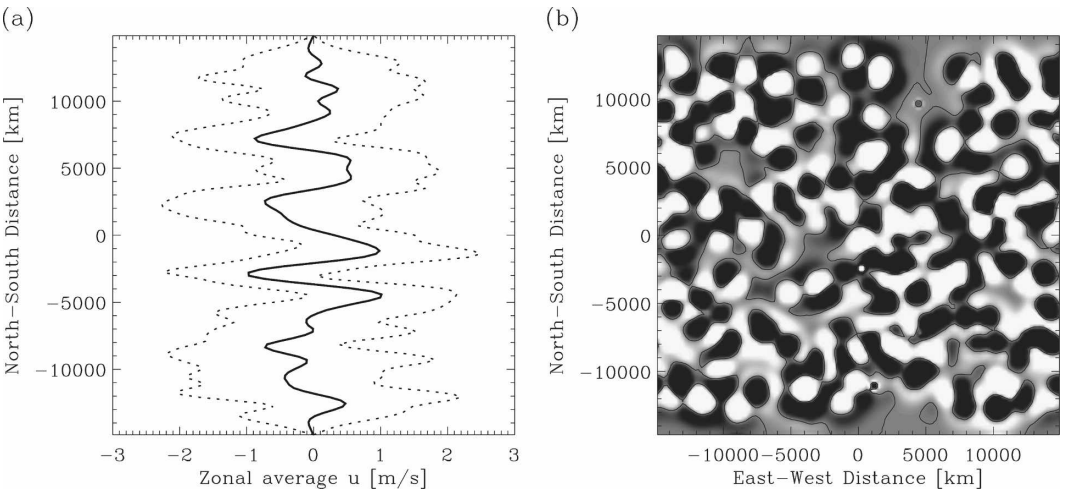

FIG. 1. Typical initial condition for the simulations, shown at the 1-bar level: (a) the initial $\overline{u}$ (solid) and $\overline{u} \pm u_{SD}$ (dotted) and (b) the initial relative vorticity field. The grayscales range from black, representing $\zeta \leq -3.0 \times 10^{-6}$ s^{-1}, to white, depicting $\zeta \geq 3.0 \times 10^{-6}$ s^{-1}, in all figures depicting ζ including this one. The contour line marks zero vorticity.

Our nominal cases use a sponge that relaxes the zonal wind component u to its zonal mean and the north–south component v to zero. We reran a few of our simulations with an alternative sponge setting in which both wind components were relaxed to zero and found that the widths and speeds of the resulting zonal jets in the active (i.e., nonsponge) layers were not significantly affected by the sponge settings. We select hyperviscosity coefficient values of $\nu_6 = 1.0 \times 10^{27}$ to 2.5×10^{27} $m^6\ s^{-1}$. These values represent the minimum necessary to stabilize the simulations, and their dissipation time scale $\Delta t \approx \nu_6^{-1}(\Delta x)^6$ is longer than 10^8 s (~1000 Earth days) for the length scale of $\Delta x \sim 1000$ km.

b. Initial conditions

Our initial conditions are generated by randomly placing numerous (between 500 and 750, depending on the simulation) small geostrophic vortices in the active simulation domain. We first construct a windless atmosphere with a constant static stability N for the entire simulation domain. We then introduce circular pressure perturbations and geostrophically balance them to create vortices. The pressure perturbation follows a Gaussian in the radial direction from the center of the vortex; thus, the wind speed is zero at the center, peaks at the characteristic radius of the pressure perturbation, and falls to zero further away. In the vertical, the pressure is perturbed such that the wind speed follows a Gaussian function of $\log p$, with a characteristic vertical scale (i.e., the "standard deviation" of the Gaussian) of H_{vortex}; thus, the characteristic thickness of a vortex becomes $2H_{vortex}$. Each vortex is circular in the horizontal with a radius of 1000 km. The vertical wind shear caused by two vertically aligned vortices produces substantial horizontal temperature gradient through the thermal wind relation; however, the situation is unphysical when it causes layer crossing. The thickness H_{vortex} and characteristic wind speed U_{vortex} of the vortices are determined so that unphysical isentropic layer crossings do not occur when a vortex is stacked on top of another of an equal U_{vortex} but with the opposite sign. In our initial conditions, we use $U_{vortex} \approx 1$ m s^{-1}, and H_{vortex} has approximately 1.5 and 0.5 scale heights for the low and high static stability cases ($N = 0.001$ and 0.005 s^{-1}), respectively. The values represent the maximum U_{vortex} and minimum H_{vortex} without crossing layers. We minimize H_{vortex} to study the vertical structure that emerges from the initial vortical wind field, in which small vortices are randomly placed in the vertical as well as the horizontal. The initial vortex heights do not violate Dritschel and de la Torre Juárez's (1996) tall-vortex stability criterion. The active (i.e., nonsponge) simulation domain heights are approximately 6.0 and 2.7 scale heights for the low and high static stability cases, respectively; thus, two vortices can be stacked up vertically in the simulation domain in both cases. The vortices span several layers in the vertical and thus are adequately resolved.

In our simulations, we ensure that the initial Rossby number is less than 0.1 everywhere so that the geostrophy does not become a poor approximation. For every simulation presented in this paper, the sign of the vortices is set randomly such that approximately half of the vortices are anticyclonic and half are cyclonic. Figure 1

illustrates a typical initial condition: Fig. 1a shows the zonal mean zonal wind $\overline{u}$ (solid) plus or minus its zonal standard deviation (dotted). The zonal standard deviation lines denote $\overline{u} \pm u_{\mathrm{SD}}$, where

$$u_{\mathrm{SD}} \equiv (\overline{u^2} - \overline{u}^2)^{1/2} \tag{4}$$

(the overbar denotes averaging over x). Figure 1b depicts the relative vorticity ζ. The vortices are placed randomly in the horizontal domain as well as the vertical, and the initial condition contains no zonal structure. We let this initial condition evolve freely in our simulations.

3. Numerical experiments

We present our numerical experiments in this section. We design our tests based on the earlier QG (Okuno and Masuda 2003; Smith 2004) and SW (Cho and Polvani 1996; Showman 2007) studies, which indicate that, under finite deformation radius L_D, the resulting flow follows (2). In 3D, the deformation radius of the flow takes the form

$$L_D \approx \frac{NH}{f}, \tag{5}$$

where H is the characteristic vertical length scale of the flow [Eq. (7.5.5) in Gill 1982]. In principle, the vertical scale is based on the dominant vertical normal mode of the flow, but observationally characterizing the vertical flow scale for Jupiter is not straightforward (see, e.g., Achterberg and Ingersoll 1989).

In this study, we use the following procedure: First, we find a simulation that produces robust zonal jets and use it as a baseline for parameter variations. Second, we vary simulation parameters to test whether the resulting flows follow behaviors similar to the earlier QG and SW results. All the simulations presented in this paper and their parameters are listed in Table 1.

a. Emergence of zonal jets

Figures 2a and 2d present the case that developed the most robust zonal jets among all our simulations. The figures depict the flow on an isentrope at the ~1-bar level of simulation $\beta 30f30$-H (see Table 1). On this isentropic layer, the pressure varies between 1390 and 1260 mb. The simulation adopts background static stability $N = 0.005\ \mathrm{s}^{-1}$ throughout the simulation domain, which is similar to the value expected for the cloud condensation levels on Jupiter (Sugiyama et al. 2006). The β-plane parameters β and f_0 are equivalent to the Jovian 30°N values. The figure shows the flow on day 500, or ~1200 Jupiter rotations of unforced evolution after the initial small-scale turbulence shown in Fig. 1. Figure 2a shows the zonal mean zonal wind $\overline{u}$ (solid line) and the zonal standard deviation of zonal wind $\overline{u} \pm u_{\mathrm{SD}}$ (dotted lines) as a function of the north–south coordinate y. The figure reveals robust zonal jets: four eastward and five westward, each of them ~2500 km wide.

Even though the initial condition contains no coherent vertical structure, the emerged jets are coherent in the vertical. Figure 3a shows $\overline{u}$ projected on the meridional plane. Note that this version of the EPIC model does not contain explicit momentum diffusion in the vertical. In the absence of heat sources, the model does not have thermal diffusion either: thus, these vertically coherent structures are due only to the flow's self-organizing nature, and not to diffusion. (Note also that in the absence of heating, numerical inaccuracies in the conservation properties—so-called "numerical diffusion"—in the vertical are minimal in isentropic coordinate models such as EPIC). In this particular simulation, the height of each jet is constrained by the depth of the simulation domain; nevertheless, the figure illustrates that vertically coherent structure can emerge from randomly placed small vortices.

These jets are extremely robust. To measure the robustness of the jets, we define the zonality of the flow as

$$Z \equiv \left| \overline{\zeta} / \zeta_{\mathrm{SD}} \right|, \tag{6}$$

which is a function of space (the north–south coordinate y and the pressure p) and time; ζ_{SD} is the zonal standard deviation of relative vorticity ζ. When the flow has little dependence on x, the relative vorticity takes the form

$$\zeta \approx -\frac{\partial u}{\partial y}; \tag{7}$$

thus, high zonality implies dominance of u over v and demonstrates the robustness of the final banded structure. Figure 3b displays the Z of simulation $\beta 30f30$-H on day 500 projected on the meridional plane. The figure shows that by day 500 some jets have achieved zonality in excess of $Z \approx 10$. The importance of considering the zonality of the flow is demonstrated by the time evolution of the flow. The time evolution of $\overline{u}$ and Z are displayed in Figs. 4a and 4b, respectively, of simulation $\beta 30f30$-H at the ~1-bar level, the same simulation at the same altitude as in Figs. 2a and 2d. Figure 4a shows that the jets appear to form relatively quickly by day 200 and undergo little subsequent change: it shows that the zonal-mean flow quickly takes the shape of the final result (by day ~200) and the extrema of $\overline{u}$ do not exhibit the merging, branching, or migrating behaviors

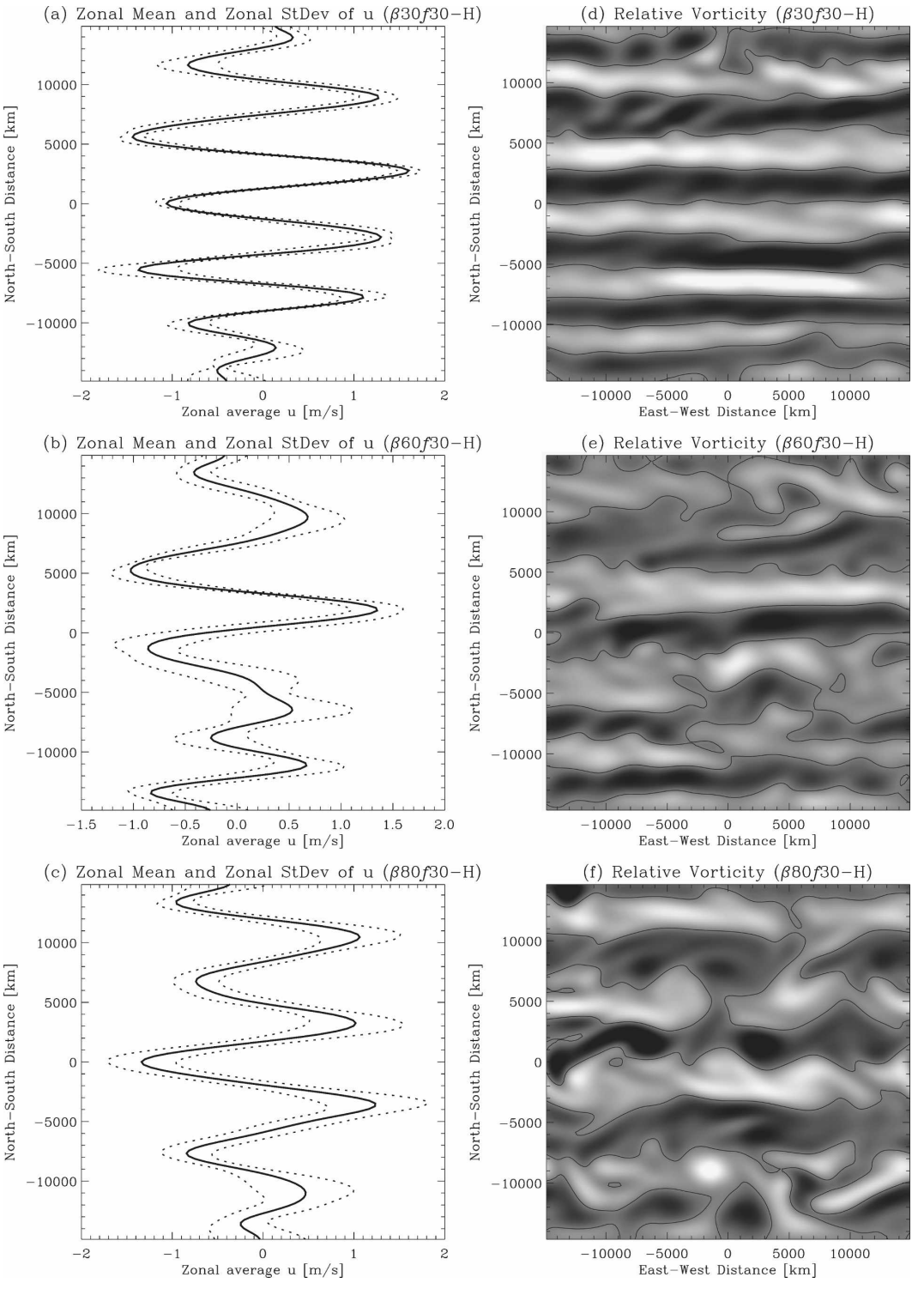

FIG. 2. Results of β sensitivity test simulations on the isentropic layer at the ~1-bar level on day 500: (left) $\overline{u}$ and $\overline{u} \pm u_{SD}$; (right) relative vorticity fields in the same format as in Fig. 1b.

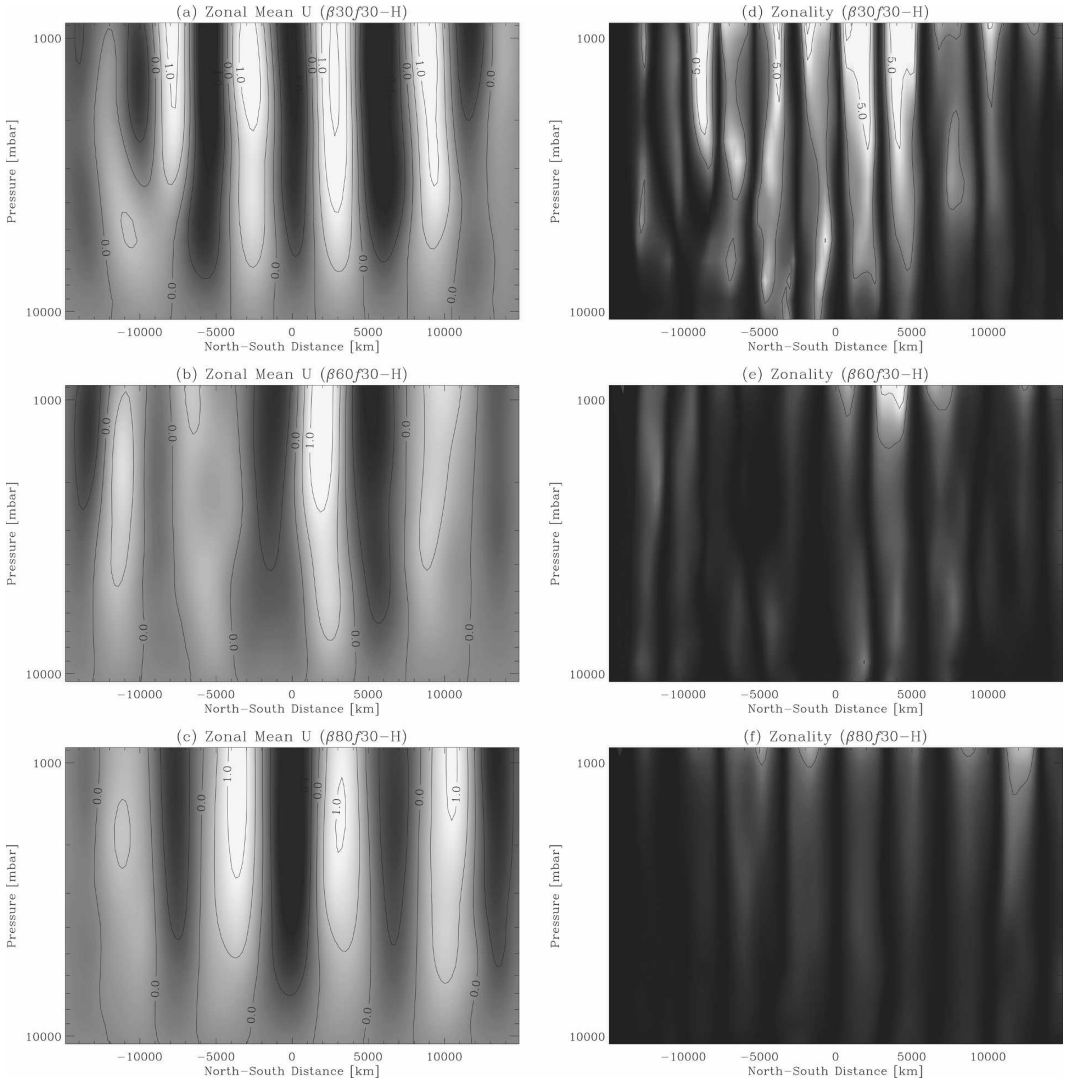

FIG. 3. Meridional projections of the wind in the β sensitivity simulations: (a)–(c) $\overline{u}$ on day 500 of the simulation; (d)–(f) Z on day 500. For (a)–(c), black and white represent $\overline{u} \leq -1.0$ m s^{-1} and $\overline{u} \geq 1.0$ m s^{-1}, respectively—the same grayscale levels are used for all meridional projections of $\overline{u}$ in the subsequent figures. The contour line spacing is 0.5 m s^{-1}. For (d)–(f), black and white represent $Z = 0.0$ and $Z \geq 5.0$, respectively, and the contour lines are drawn every 2.5 units (lines are not drawn for $Z > 10.0$ to enhance readability).

that have been shown for jets in past studies (e.g., Panetta 1993; Huang and Robinson 1998). However, the zonality of the flow shown in Fig. 4b indicates that the jets continue to evolve throughout the >1000-day simulation duration.

Another important attribute of a robust zonal jet is the dominance of the zonal wind u over the meridional component v. The resulting flow of $\beta 30f30$-H attains this characteristic as illustrated in Fig. 2b, in which the relative vorticity field exhibits a clear banded structure. Also, the time evolution of Z shown in Fig. 4b clearly illustrates that the wind shear becomes dominated by the meridional variations of u rather than the zonal variations in v. These flow features are typical of the outcomes categorized as "zonal jets" in Table 1 in the column headed "Resulting flow."

Jupiter's jets show two remarkable qualities, robustness and sharpness—the latter referring to peak curvatures that exceed β and hence violate the barotropic stability criterion $-\partial\overline{\zeta}/\partial y < \beta$. The jets that emerge in these simulations only reproduce the first characteristic; they are long-lived and quite stable, but they are not sharper than β and do not violate the barotropic stability criterion. Figure 5a shows the negative zonally averaged gradient of the relative vorticity on an isentropic layer at the ~1-bar level for $\beta 30f30$-H and its

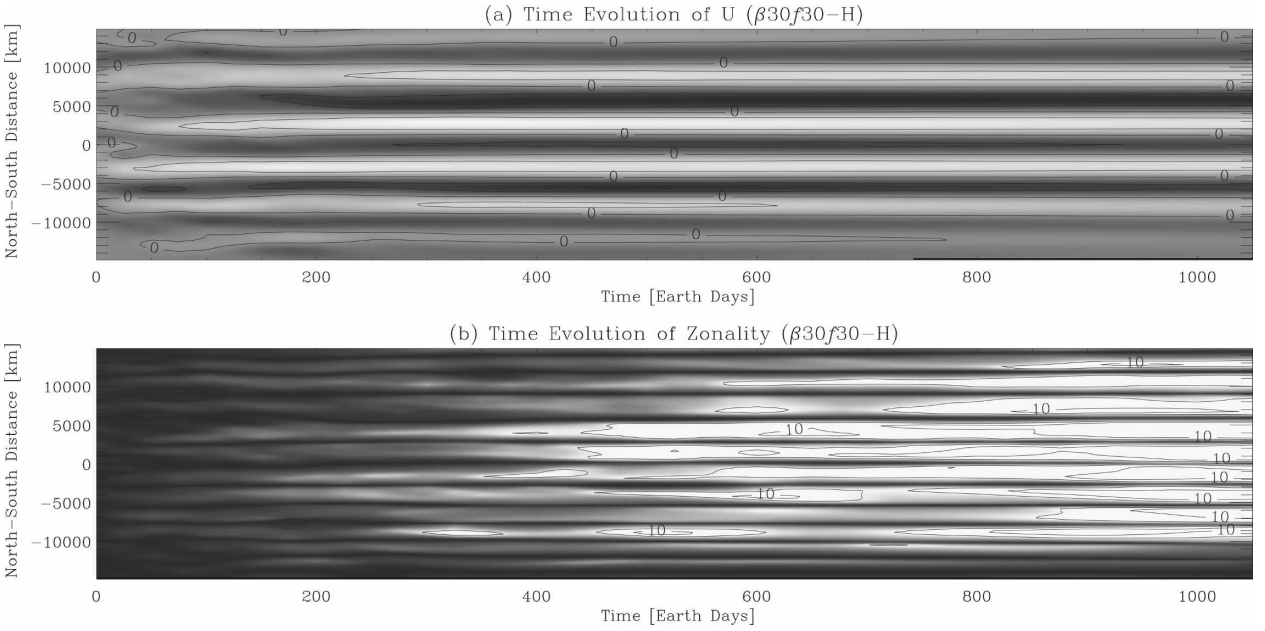

FIG. 4. Time evolution of the nominal case $\beta 30f30$-H on the isentrope at ~1 bar. (a) The evolution of u, which shows little change after day 200. The grayscales range from −1.0 (black) to 1.0 m s^{-1} (white), with a contour line drawn every 1.0 m s^{-1}. (b) The zonality Z. Black is $Z = 0.0$ and white is $Z \geq 5$; contour lines are drawn every 5.0 up to $Z = 10.0$.

zonal standard deviation. The figure also shows β for the simulation (dashed) and illustrates that $-\partial\zeta/\partial y$ is a factor of 2 too small to violate the criterion. This result agrees with 2D turbulence investigations that also produce jets satisfying the criterion (e.g., Williams 1978; Maltrud and Vallis 1993; Cho and Polvani 1996; Nozawa and Yoden 1997; Huang and Robinson 1998). To further illustrate the resulting flow, we display the potential vorticity (PV) in Figs. 5b and 5c. Figure 5b shows the zonal mean plus or minus the zonal standard deviation of PV; Fig. 5c displays the map of PV.

Even though the flows continue to evolve throughout the >1000-day simulations, we terminate the simulations around day 1000, after which the dynamics at the small length scales begin to be affected by the numerical stability terms. As discussed earlier, the characteristic time scale of hyperviscosity at the 1000-km length scale is on the order of 10^3 days. Also, because our flows are unforced, the kinetic energy continues to redistribute in the spectral space, even though there may be scales at which the energy flow is slowed, such as the Rhines length and the deformation radius. When a system is forced at the small scale and damped at large scales, the energy continuously cascades through the spectral space, and the system reaches an equilibrium when the energy source is balanced by the dissipation. In contrast, our system has no energy input; thus, we do not expect the flow to reach an equilibrium until all kinetic energy is dissipated.

b. *Sensitivity to planetary vorticity gradient* β

Treating run $\beta 30f30$-H as a baseline result, we now vary its β-plane parameters to test the behaviors of the resulting flows. Equation (2) shows that L'_β becomes imaginary when $L_\beta \gtrsim L_D$, and under such conditions, SW studies suggest that the spectral redistribution of the kinetic energy leads to a vortex-dominated flow (Showman 2007; Scott and Polvani 2007). Thus, we first test the sensitivity of the flows to L_β by varying β only. If the resulting flow follows a dynamics similar to that in the shallow-water experiments, we expect the resulting flow to become more vortex dominated with decreasing β. This test is equivalent to varying the planetary radius without changing the planetary rotation rate, except that our β-plane experiments exclude the curvature effects of a real planet. This sensitivity test consists of the simulations $\beta 15f30$-H, $\beta 30f30$-H, $\beta 60f30$-H, and $\beta 80f30$-H, which have values of β representative of Jovian 15°, 30°, 60°, and 80°N, respectively, without changing the background Coriolis parameter f_0. Note that β decreases with latitude, and thus L_β increases with increasing latitude. For a full list of parameters, see Table 1.

Our simulation results show that the flow becomes more vortex dominated as L_β is increased through varying β, which is consistent with previous QG and SW results. Figure 2 illustrates our result, showing the flows at the ~1-bar level on day 500 of the β sensitivity test

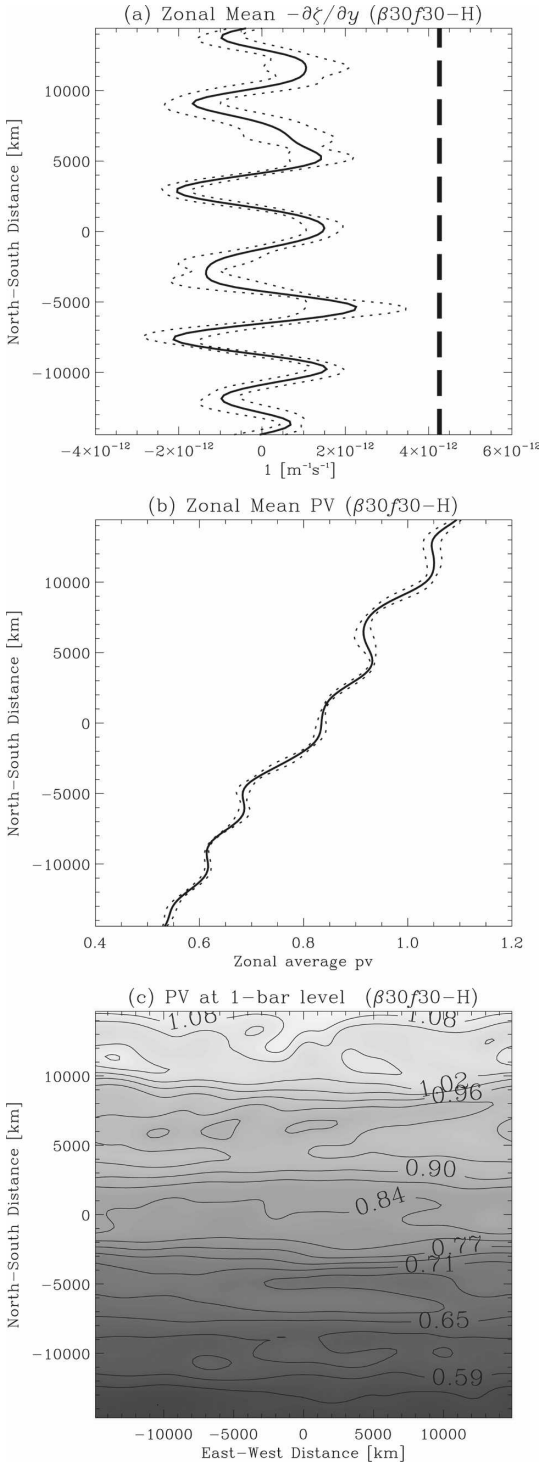

FIG. 5. $\beta 30f30$-H's vorticities on day 500 on the ~1-bar isentropic layer. (a) The north–south gradient of the relative vorticity $\partial\zeta/\partial\zeta$ (solid) and its zonal standard deviation (dotted). The thick dashed line indicates $\beta = 4.26 \times 10^{-12}$ m^{-1} s^{-1}, the value used for the simulation. It shows that the resulting flow does not violate the barotropic stability criterion. (b) The PV (solid) and its zonal standard deviation (dotted) as a function of latitude. (c) PV on the isentrope. The unit of PV in (b) and (c) is 10^{-7} K Pa^{-1} m^{-1} s^{-1}.

simulations. Figures 2a–c and 2d–f show the $\overline{u}$ and relative vorticity for the simulations, respectively. The nominal case $\beta 30f30$-H (shown in Figs. 2a and 2d) led to a flow dominated by robust zonal jets, as already discussed. The simulation $\beta 15f30$-H also resulted in a jet-dominated flow (not shown). Zonal features are weak in $\beta 60f30$-H (Figs. 2b and 2e) except for the strong eastward and westward jets at $y \approx 2500$ and 5000 km, respectively—this is an example of a flow identified as "vortices between zonal jets" in Table 1. For $\beta 80f30$-H, plotting $\overline{u}$ (Fig. 2c) gives an impression that the experiment led to multiple zonal jets; however, the relative vorticity field (Fig. 2f) reveals that the zonal flows, while still exhibiting banded structure, exhibit substantial zonal variation and contain many vortices. Although the wind field is vortex dominated in $\beta 80f30$-H, cyclonic (anticyclonic) vortices align in a cyclonic (anticyclonic) zone and help maintain the banded structure: we identify such flows as "vortices with zonal flow" in Table 1. The meridional cross sections of the flows also clearly show that reducing β leads to flows that are less jet dominated. Although the $\overline{u}$ of all three cases shown in Figs. 3a–c may resemble zonal jets, their zonalities Z (Figs. 3d–f) clearly indicate the loss of zonal features with decreasing β in the simulations.

We further characterize the resulting flows by comparing the zonal and eddy components of the kinetic energy. In 3D compressible flow, the total kinetic energy is

$$K = \int \frac{\rho}{2}(u^2 + v^2)\, dV$$

$$= \int \frac{\rho}{2}(\overline{u}^2 + 2\overline{u}u' + u'^2 + \overline{v}^2 + 2\overline{v}v' + v'^2)\, dV, \quad (8)$$

where the integration is over the whole volume domain. In the second line, we decomposed the velocity components into the zonal mean and the deviation from the zonal mean ($u \equiv \overline{u} + u'$ and $v \equiv \overline{v} + v'$). We neglect the vertical flow component because it is much smaller than the horizontal ones in a hydrostatic atmosphere. The horizontal variations in ρ are small in all of our simulations, and as a result, the contribution of the "cross terms," $\int \rho(\overline{u}u' + \overline{v}v')dV$, is at least four orders of magnitude smaller than the other terms in all our simulations. This is a direct consequence of weak divergence in our flow due to the slow winds. Thus, for our simulations, we define the zonal and eddy components of the kinetic energy as

$$\mathrm{KZ} = \int \frac{\rho}{2}(\overline{u}^2 + \overline{v}^2)\, dV \quad \text{and} \quad (9)$$

$$\mathrm{KE} = \int \frac{\rho}{2}(u'^2 + v'^2)\, dV, \quad (10)$$

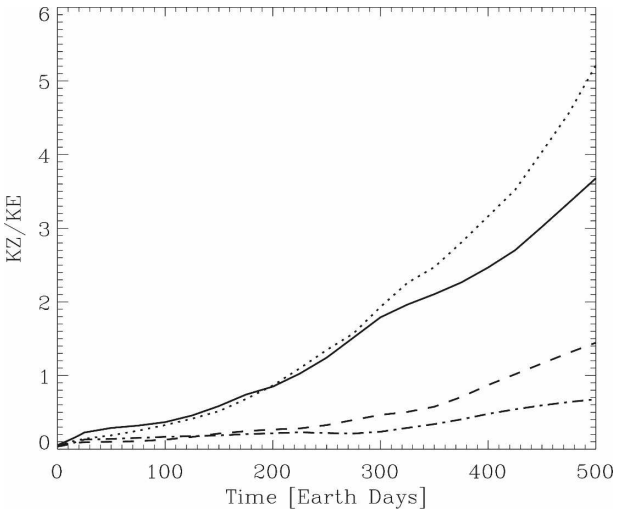

FIG. 6. KZ/KE vs time for the β sensitivity test simulations. The solid, dotted, dashed, and dotted–dashed lines depict the simulations $\beta 15f30$-H, $\beta 30f30$-H, $\beta 60f30$-H, and $\beta 80f30$-H, respectively.

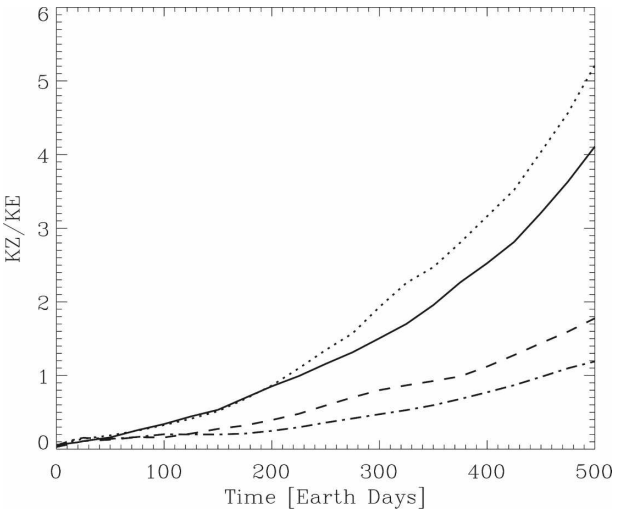

FIG. 7. KZ/KE vs time for the f sensitivity test simulations. The solid, dotted, dashed, and dotted–dashed lines depict the simulations $\beta 30f15$-H, $\beta 30f30$-H, $\beta 30f60$-H, and $\beta 30f80$-H, respectively.

respectively. Figure 6 compares the time evolution of KZ/KE for all β sensitivity test simulations. Here, the volume integration is taken over the whole active model domain excluding the sponge layers. It clearly demonstrates that KZ/KE grows substantially faster in the two simulations that led to jet-dominated flows ($\beta 15f30$-H and $\beta 30f30$-H) than in the flows that resulted in more vortical activities ($\beta 60f30$-H and $\beta 80f30$-H) and highlights the difference between those flow regimes.

c. Sensitivity to the Coriolis parameter f_0

We now test the flow's sensitivity to f_0. Our intention is to vary only the deformation radius L_D without affecting L_β. As in the sensitivity test for β, this follows earlier SW and QG studies. We expect the flow to become more vortex dominated when L_D is decreased by increasing f_0 while keeping L_β constant. We fix the value of β equal to that of the run $\beta 30f30$-H, and vary only f_0 in this test. This sensitivity test consists of the simulations $\beta 30f15$-H, $\beta 30f30$-H, $\beta 30f60$-H, and $\beta 30f80$-H, which have values of f_0 representative of Jovian 15°, 30°, 60°, and 80°N, respectively. The result of this test reveals that zonal features weaken as L_D is decreased by increasing f_0. Figure 7 shows the time evolution of KZ/KE for the f_0 sensitivity test simulations. As in the β sensitivity test, the two simulations that led to jet-dominated results have substantially faster growth of KZ/KE than the other two cases with larger f_0, which resulted in more vortical flows.

d. Simulations with 15°, 30°, 60°, and 80°N central latitudes, and their sensitivity to static stability N

Now, we compare simulations with the β-plane parameters that represent 15°, 30°, 60°, and 80°N latitudes on Jupiter. We also vary the Brunt–Väisälä frequency N to test its effect. The motivation for varying N is similar to the sensitivity test of f_0: we attempt to vary only the deformation radius L_D without affecting L_β. To test the effect of N, we reduce the static stability of the four $N = 0.005\ \mathrm{s}^{-1}$ simulations to $N = 0.001\ \mathrm{s}^{-1}$. The simulations are listed under "Latitude sensitivity test" in Table 1. Note that the vertical layer spacing Δz for the $N = 0.001\ \mathrm{s}^{-1}$ simulations is greater than in the high static stability cases, and, in the geometric sense, their vertical resolution is lower. However, as discussed earlier, we keep the vertical resolution consistent by keeping $\Delta z/\Delta x < 3f/N$, and in this sense the vertical resolutions of all our simulations are comparable.

We again compare the time evolution of KZ/KE, shown in Fig. 8. Again, the simulations that produced jet-dominated flows ($\beta 15f15$-H, $\beta 30f30$-H, and $\beta 15f15$-L) exhibit substantially faster growth of KZ/KE. Also, comparing simulations with the same "latitude" reveals that KZ/KE is higher for the high static stability cases than their low-N counterparts, with the exception of the 15°N cases. The low static stability 80°N case ($\beta 80f80$-L) resulted in an especially vortex-dominated flow (as shown in Fig. 9), which contains no discernible zonal structure—this is an example of "vortex dominated" flows listed in Table 1.

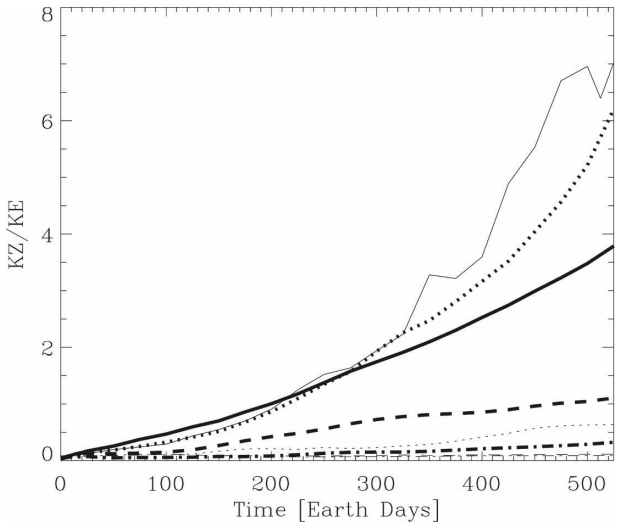

FIG. 8. KZ/KE vs time for the latitude–sensitivity test simulations. The thick and thin lines denote results for the $N = 0.005\ s^{-1}$ and $N = 0.001\ s^{-1}$ cases, respectively. The solid, dotted, dashed, and dotted–dashed lines depict the simulations with β and f_0 tuned to equivalent of Jupiter's 15°, 30°, 60°, and 80°N conditions, respectively.

e. Effects of L_β and L_D on zonal jet formation

We now analyze the relation between L_β and L_D in all 18 simulations listed in Table 1 and study its effect. The result is summarized in Fig. 10, which shows that zonal jets form in simulations when L_β is substantially less than L_D, as predicted by (2). As remarked in Table 1, we call a flow feature a jet when it satisfies both $Z > 2.5$ and $|\overline{u}| > 0.5\ m\ s^{-1}$. In the plot, $L_\beta = \sqrt{U/\beta}$ where $U = \sqrt{2K/M}$; M and K are the total mass of air and the total kinetic energy, respectively, in the active simulation domain. The deformation radius plotted here is the first baroclinic radius in each simulation. To calculate the first baroclinic radius, we follow the normal mode decomposition procedure of Achterberg and Ingersoll (1989) to numerically solve the eigenvalue problem on our model grid in the vertical. Thus, each data point in Fig. 10 corresponds to a simulation in Table 1. The figure illustrates that the boundary between the domains of jets and vortical flows roughly follows the line of $L_\beta = L_D$.

4. Vertical and horizontal jet scales

In this section, we examine the vertical structures of the resulting jets using deeper simulation domains without changing other simulation parameters. Simulations $\beta 30f15$-D, $\beta 30f30$-D, $\beta 30f60$-D, and $\beta 30f80$-D have parameters identical to $\beta 30f15$-H, $\beta 30f30$-H, $\beta 30f60$-H, and $\beta 30f80$-H, respectively, except that their simulation domains extend deeper, placing the abyssal layer at the 100-bar level. This test also examines the sensitivity of our results to the domain depths. In terms of jet versus vortex domination in the resulting flows, all four cases produced outcomes consistent with the corresponding shallow simulations. The simulation $\beta 30f80$-D will not be further discussed because it produced a largely vortex-dominated flow, as expected. These deep simulations developed many jets whose heights are much shorter than the simulation domain. Figure 11 shows the meridional cross sections of $\overline{u}$ on day 500 of the simulations $\beta 30f15$-D, $\beta 30f30$-D, and $\beta 30f60$-D and reveals that the height of the jets become taller with greater f.

We analyze the relationship between the jet heights

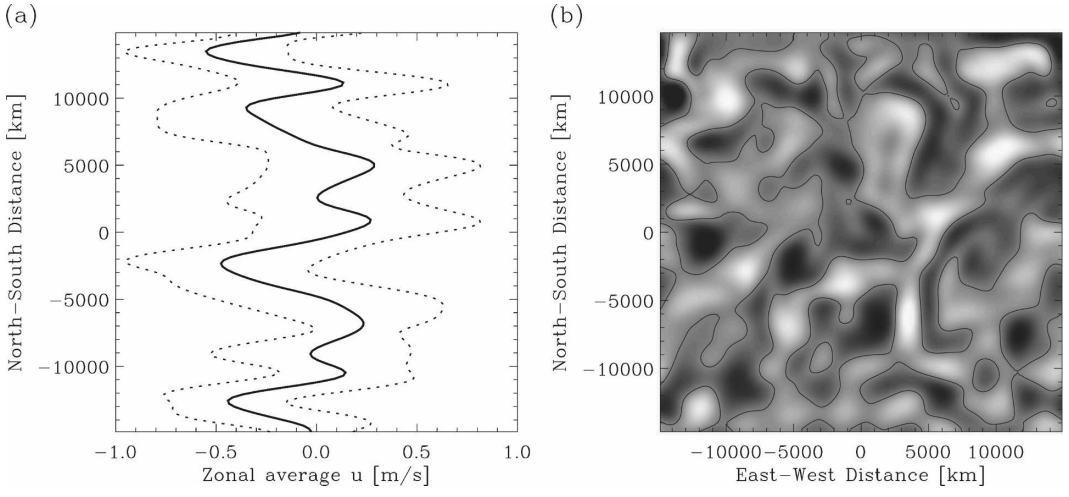

FIG. 9. Same as Fig. 1 but for day 500 of $\beta 80f80$-L.

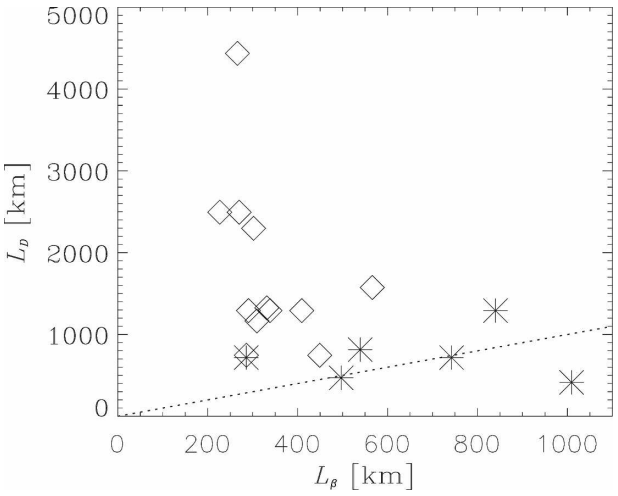

FIG. 10. The relationship between L_β and L_D. Each data point corresponds to a simulation in Table 1. The diamonds represent the simulations that produced at least one zonal jet, and the asterisks denote the cases that became vortex-dominated. The dotted line marks $L_\beta = L_D$.

$H_{\rm Jet}$ and widths $L_{\rm Jet}$ and present the result in Fig. 12. The figure shows a clear trend for $H_{\rm Jet}/L_{\rm Jet}$ to grow with f/N. The figure depicts the 17 (7 eastward and 10 westward) jets that achieve $Z > 5$ and $\overline{u} > |0.5|$ m s^{-1} in the three deep-domain simulations. The widths correspond to the width of the region where the jet speed exceeds $\overline{u} > |0.5|$ m s^{-1}. The heights are measured by integrating the temperature-dependent scale height ($H \equiv RT/g$, where R is the specific gas constant and T is the temperature) in the vertical across the region of $\overline{u} > |0.5|$ m s^{-1}; when this region reaches the 1-bar level, we treat the 1-bar level as the top. Figure 11 shows the $H_{\rm Jet}/L_{\rm Jet} = f/N$ line as a reference and illustrates that our $H_{\rm Jet}/L_{\rm Jet}$ data points follow f/N within a factor of ~2. The eastward (westward) jets are marked by diamonds (asterisks) in the figure; the results indicate no notable difference in the behaviors between the eastward and westward jets. The scatter of $H_{\rm Jet}/L_{\rm Jet}$ becomes larger at high f/N probably because the heights of some jets in $\beta 30f60$-D are constrained by the simulation domain.

5. Discussion

We have tested whether self-organization of 3D stratified geostrophic flow under the influence of β can produce zonal jets from initial small-scale turbulence without forcing. Our results (presented in section 3a) show that extremely robust zonal jets can emerge from such initial conditions. The zonal jets produced in our simulations exhibit very little variation in the zonal di-

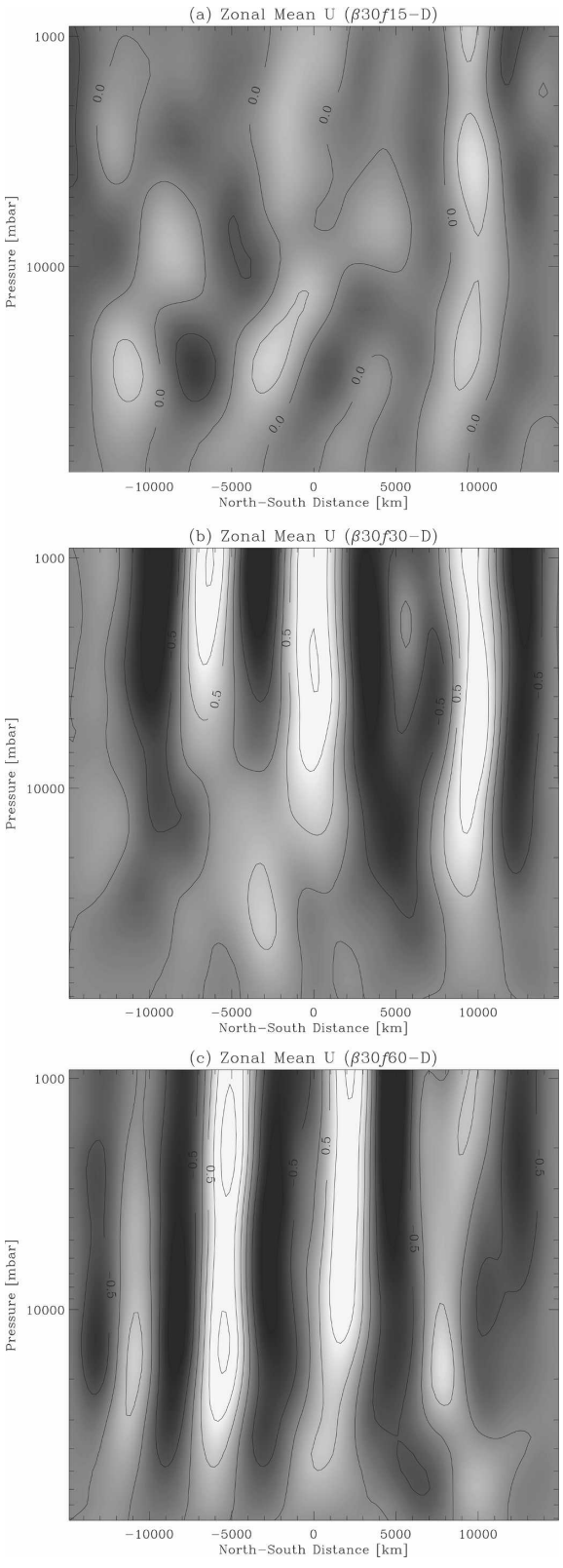

FIG. 11. Values of $\overline{u}$ for the deep-domain simulations on day 500. The grayscale values and contour line spacings are the same as in Fig. 3 for $\overline{u}$.

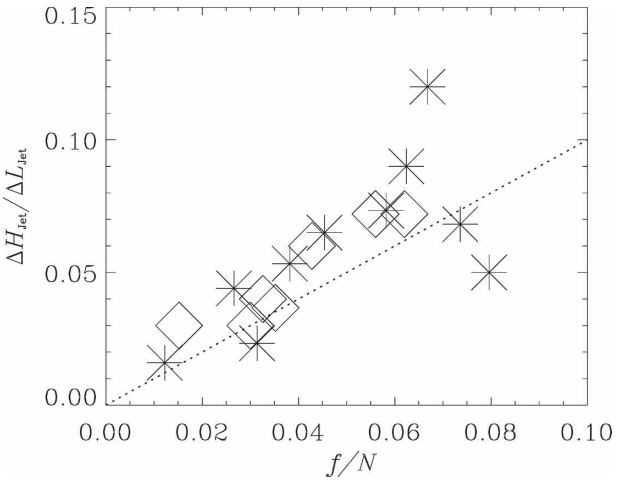

FIG. 12. The relationship of the height-to-width ratio of the zonal jets that emerged in the deep-domain simulations presented in Fig. 11 to f/N. The diamonds (asterisks) are the eastward (westward) zonal jets that satisfy both $|\overline{u}| > 0.5$ m s^{-1} and $Z > 2.5$. The figure reveals that the jets' height-to-width ratio $\Delta H_{\rm Jet}/\Delta L_{\rm Jet}$ closely follows f/N.

rection. The zonal jets are steady in time as well, and the peaks of the jets exhibit no meandering or merging after they stabilize around day 200 of the simulations. None of the jets in our simulations become unstable or weaken after they form. These jets do not violate the barotropic stability criterion; however, the nonviolation here may be a result of the slow wind speeds and we do not imply that this is an inherent limitation of the mechanism that leads to the formation of the zonal jets in our study.

We then test the flow's sensitivities to the Coriolis parameter f_0, its meridional gradient β, and the static stability N in sections 3b–d, using values of β and f representative of the conditions on Jupiter. Our results are consistent with the idea that the outcome of the flow's turbulent self-organization transitions from a jet-dominated regime in $L_\beta \lesssim L_D$ to an isotropic turbulence in $L_\beta \gg L_D$, as demonstrated in section 3e. Our result, produced using a 3D model, is consistent with the suppression of the Rhines effect under a small deformation radius demonstrated in one-layer quasigeostrophic (Okuno and Masuda 2003; Smith 2004; Theiss 2004) and SW (Cho and Polvani 1996; Showman 2007; Scott and Polvani 2007) systems. Our simulations demonstrate that the parameters that determine L_β and L_D have strong control over whether resulting flow becomes dominated by zonal jets or vortices. To our knowledge, this is the first systematic study that examines the conditions of zonal jet formation from initial small-scale turbulence for 3D stratified geostrophic turbulence. However, the mechanism that determines the widths of the jets in our results remains unclear. Our simulations reveal no systematic variation in the jet width in our sensitivity tests.

Our simulations showed that when zonal jets form, their structure can become coherent in the vertical even though the initial conditions have no vertically aligned structure. The mechanism of forming vertically coherent features, or the barotropization of the flow, has been discussed by, for example, Rhines (1979), Salmon (1998), and Galperin et al. (2006), and in the Jupiter context by Showman et al. (2006) and Lian and Showman (2008). Their studies show that baroclinic instabilities are responsible for the flow barotropization; however, our unforced study lacks baroclinic instability. Charney (1971) demonstrated that in 3D geostrophic turbulence, energy transfer toward higher wavenumbers is inhibited whereas the inverse transfer is not restricted. The mechanism that leads to the vertically coherent structures shown in Figs. 3 and 10 seems to be a result of this upscale energy transfer in the vertical as well as in the horizontal dimensions.

Our results also illustrate that the height-to-width ratio of the resulting zonal jets closely follows f/N when the jets' heights are not restricted by the simulation domain. This is consistent with the theory that QG flows are invariant when the vertical scale is normalized by f/N (Charney 1971; reviewed by Haynes 2005). Our result is analogous to that of the height-to-radius ratio $H_{\rm vortex}/L_{\rm vortex}$ of stable QG vortices, which also scales with f/N (Dritschel and de la Torre Juárez 1996; Dritschel et al. 1999; Reinaud et al. 2003; Dritschel et al. 2005). Experiments of stratified turbulence in a rotating tank by Praud et al. (2006) show similar results. Numerical simulations of stratified geostrophic turbulence by Waite and Bartello (2006) show that the ratio of characteristic vertical and horizontal flow scales also follow f/N (they do not obtain zonal jets). Our result establishes that the f/N scaling applies to jets formed by geostrophic turbulence in 3D. Combined, our result on jets and the earlier studies of vortices suggest that the f/N height-to-width ratio holds for both vortices and jets in 3D geostrophic flows, at least for unforced cases. Although it is not surprising that the jets in our results follow this scaling, it is assuring to find that the f/N law applies to both vortices and jets.

We also note that when vortices are embedded between zonal jets, the vortex heights are shorter than those of the jets. The radii of these vortices are smaller than the width of the jets. We do not measure the height-to-radius ratio for the vortices because a cyclonic (anticyclonic) vortex is usually embedded in a cyclonic (anticyclonic) shear zone and unambiguously defining the height and radius of a vortex is difficult.

Nevertheless, it is possible that the vortices and jets independently follow the f/N vertical-to-horizontal scaling ratio. Earlier one-layer model studies, which seem to have difficulties in producing vortices embedded between zonal jets, do not take account of multiple baroclinic modes, and jets and vortices are forced to have the same vertical scale. As suggested by Showman (2007), our study hints that including multiple baroclinic modes may be important in simultaneously reproducing both jets and vortices as in the Jovian atmospheres.

A major constraint in our study's approach is the total kinetic energy that can be physically contained in the initial small-scale turbulence. Although we succeeded in producing slow, robust zonal jets, this limitation prevented us from studying fast zonal jets with speeds approaching those of Jupiter. Our study suggests that to generate Jupiter-like *fast* zonal jets in 3D from small-scale vorticity sources the flow must be continuously forced; this will be a topic of future investigations.

Acknowledgments. KMS acknowledges useful inputs from Boris Galperin, Peter Read, Hiro Yamazaki, and Shi-geo Yoden. The authors thank constructive comments by two anonymous reviewers. The study was supported by NASA Planetary Atmospheres Grants NNG06GF28G (to APS) and NNG05GO06G (to TED).

REFERENCES

Achterberg, R. K., and A. P. Ingersoll, 1989: A normal-mode approach to Jovian atmospheric dynamic. *J. Atmos. Sci.,* **46,** 2448–2462.

Batchelor, G. K., 1953: *The Theory of Homogeneous Turbulence.* Cambridge University Press, 197 pp.

Charney, J. G., 1971: Geostrophic turbulence. *J. Atmos. Sci.,* **28,** 1087–1095.

Chekhlov, A., S. A. Orszag, S. Sukoriansky, B. Galperin, and I. Staroselsky, 1996: The effect of small-scale forcing on large-scale structures in two-dimensional flows. *Physica D,* **98,** 321–334.

Cho, J. Y.-K., and L. M. Polvani, 1996: The emergence of jets and vortices in freely evolving, shallow-water turbulence on a sphere. *Phys. Fluids,* **8,** 1531–1552.

Danilov, S., and V. M. Gryanik, 2004: Barotropic beta-plane turbulence in a regime with strong zonal jets revisited. *J. Atmos. Sci.,* **61,** 2283–2295.

——, and D. Gurarie, 2004: Scaling, spectra, and zonal jets in beta-plane turbulence. *Phys. Fluids,* **16,** 2592–2603.

Dowling, T. E., A. S. Fischer, P. J. Gierasch, J. Harrington, R. P. Lebeau, and C. M. Santori, 1998: The explicit planetary isentropic coordinate (EPIC) atmospheric model. *Icarus,* **132,** 221–238.

Dritschel, D. G., and M. de la Torre Juárez, 1996: The instability and breakdown of tall columnar vortices in a quasi-geostrophic fluid. *J. Fluid Mech.,* **328,** 129–160.

——, ——, and M. H. P. Ambaum, 1999: The three-dimensional vortical nature of atmospheric and oceanic turbulent flows. *Phys. Fluids,* **11,** 1512–1520.

——, R. K. Scott, and J. N. Reinaud, 2005: The stability of quasi-geostrophic ellipsoidal vortices. *J. Fluid Mech.,* **536,** 401–421.

Galperin, B., S. Sukoriansky, N. Dikovskaya, P. L. Read, Y. H. Yamazaki, and R. Wordsworth, 2006: Anisotropic turbulence and zonal jets in rotating flows with a β-effect. *Nonlinear Processes Geophys.,* **13,** 83–98.

Gill, A. E., 1982: *Atmosphere–Ocean Dynamics.* Academic Press, 662 pp.

Haynes, P., 2005: Stratospheric dynamics. *Annu. Rev. Fluid Mech.,* **37,** 263–293.

Huang, H.-P., and W. A. Robinson, 1998: Two-dimensional turbulence and persistent zonal jets in a global barotropic model. *J. Atmos. Sci.,* **55,** 611–632.

——, B. Galperin, and S. Sukoriansky, 2001: Anisotropic spectra in two-dimensional turbulence on the surface of a rotating sphere. *Phys. Fluids,* **13,** 225–240.

Iacono, R., M. V. Struglia, and C. Ronchi, 1999: Spontaneous formation of equatorial jets in freely decaying shallow water turbulence. *Phys. Fluids,* **11,** 1272–1274.

Kitamura, Y., and Y. Matsuda, 2004: Numerical experiments of two-level decaying turbulence on a rotating sphere. *Fluid Dyn. Res.,* **34,** 33–57.

Lian, Y., and A. P. Showman, 2008: Deep jets on gas-giant planets. *Icarus,* **194,** 597–615.

Limaye, S. S., 1986: Jupiter: New estimates of the mean zonal flow at the cloud level. *Icarus,* **65,** 335–352.

Maltrud, M. E., and G. K. Vallis, 1993: Energy and enstrophy transfer in numerical simulations of two-dimensional turbulence. *Phys. Fluids,* **5,** 1760–1775.

Nozawa, T., and S. Yoden, 1997: Formation of zonal band structure in forced two-dimensional turbulence on a rotating sphere. *Phys. Fluids,* **9,** 2081–2093.

Okuno, A., and A. Masuda, 2003: Effect of horizontal divergence on the geostrophic turbulence on a beta-plane: Suppression of the Rhines effect. *Phys. Fluids,* **15,** 56–65.

Panetta, R. L., 1993: Zonal jets in wide baroclinically unstable regions: Persistence and scale selection. *J. Atmos. Sci.,* **50,** 2073–2106.

Porco, C. C., and Coauthors, 2003: Cassini imaging of Jupiter's atmosphere, satellites, and rings. *Science,* **299,** 1541–1547.

Praud, O., J. Sommeria, and A. M. Fincham, 2006: Decaying grid turbulence in a rotating stratified fluid. *J. Fluid Mech.,* **547,** 389–412.

Reinaud, J. N., D. G. Dritschel, and C. R. Koudella, 2003: The shape of vortices in quasi-geostrophic turbulence. *J. Fluid Mech.,* **474,** 175–192.

Rhines, P. B., 1975: Waves and turbulence on a beta-plane. *J. Fluid Mech.,* **69,** 417–443.

——, 1979: Geostrophic turbulence. *Annu. Rev. Fluid Mech.,* **11,** 401–441.

——, 1994: Jets. *Chaos,* **4,** 313–339.

Salmon, R., 1998: *Lectures on Geophysical Fluid Dynamics.* Oxford University Press, 378 pp.

Scott, R. K., and L. M. Polvani, 2007: Forced-dissipative shallow-water turbulence on the sphere and the atmospheric circulation of the giant planets. *J. Atmos. Sci.,* **64,** 3158–3176.

Showman, A. P., 2007: Numerical simulations of forced shallow-water turbulence: Effects of moist convection on the large-scale circulation of Jupiter and Saturn. *J. Atmos. Sci.,* **64,** 3132–3157.

——, P. J. Gierasch, and Y. Lian, 2006: Deep zonal winds can result from shallow driving in a giant-planet atmosphere. *Icarus,* **182,** 513–526.

Smith, K. S., 2004: A local model for planetary atmospheres forced by small-scale convection. *J. Atmos. Sci.,* **61,** 1420–1433.

Sugiyama, K., M. Odaka, K. Kuramoto, and Y.-Y. Hayashi, 2006: Static stability of the Jovian atmospheres estimated from moist adiabatic profiles. *Geophys. Res. Lett.,* **33,** L03201, doi:10.1029/2005GL024554.

Sukoriansky, S., N. Dikovskaya, and B. Galperin, 2007: On the arrest of inverse energy cascade and the Rhines scale. *J. Atmos. Sci.,* **64,** 3312–3327.

Theiss, J., 2004: Equatorward energy cascade, critical latitude, and the predominance of cyclonic vortices in geostrophic turbulence. *J. Phys. Oceanogr.,* **34,** 1663–1678.

Vasavada, A. R., and A. P. Showman, 2005: Jovian atmospheric dynamics: An update after *Galileo* and *Cassini*. *Rep. Prog. Phys.,* **68,** 1935–1996.

Waite, M. L., and P. Bartello, 2006: The transition from geostrophic to stratified turbulence. *J. Fluid Mech.,* **568,** 89–108.

Williams, G. P., 1978: Planetary circulations. Part I: Barotropic representation of Jovian and terrestrial turbulence. *J. Atmos. Sci.,* **35,** 1399–1426.

——, 2003: Jovian dynamics. Part III: Multiple, migrating, and equatorial jets. *J. Atmos. Sci.,* **60,** 1270–1296.

Yoden, S., and M. Yamada, 1993: A numerical experiment on two-dimensional decaying turbulence on a rotating sphere. *J. Atmos. Sci.,* **50,** 631–644.

——, K. Ishioka, Y.-Y. Hayashi, and M. Yamada, 1999: A further experiment on two-dimensional decaying turbulence on a rotating sphere. *Nuovo Cimento,* **22C,** 803–812.